

**Quantitative rescattering theory of high-order harmonic generation for polyatomic molecules**Anh-Thu Le,<sup>1</sup> R. R. Lucchese,<sup>2</sup> and C. D. Lin<sup>1</sup><sup>1</sup>*Department of Physics, Cardwell Hall, Kansas State University, Manhattan, Kansas 66506, USA*<sup>2</sup>*Department of Chemistry, Texas A&M University, College Station, Texas 77843-3255, USA*

(Received 22 March 2013; published 7 June 2013)

We report applications of the quantitative rescattering theory (QRS) for calculation of high-order-harmonic generation (HHG) from polyatomic molecules in ultrashort linearly polarized intense laser pulses, using the example of the  $\text{CCl}_4$  molecule. In particular, we present a detailed analysis and a treatment for the phase of the electron returning wave packet, which recollides with the parent molecular ion to emit high-energy photons. Our results show that Cooper-type minimum structures in the molecular photoionization cross section lead to quite distinguishable minima in the HHG spectra, even for unaligned polyatomic molecules.

DOI: [10.1103/PhysRevA.87.063406](https://doi.org/10.1103/PhysRevA.87.063406)

PACS number(s): 33.80.Eh, 42.65.Ky

**I. INTRODUCTION**

High-order-harmonic generation (HHG) has been studied extensively both experimentally and theoretically over the past two decades. HHG can serve as a coherent extreme ultraviolet (XUV) and soft x-ray source, and currently, it is used as the only source for attosecond pulses [1–3]. HHG has also been shown to carry information about the targets [4–6]. Indeed, HHG spectroscopy has proved to be very promising for revealing various types of structural information about atoms and simple linear molecules [4,5,7–13], such as internuclear distance, symmetry of the highest occupied molecular orbital (HOMO) or even the HOMO wave function, and the photoionization transition dipole. Recent experiments have now started to focus on polyatomic molecules [14–17]. However, for HHG spectroscopy to become a practical tool for polyatomic targets, a solid theoretical method needs to be established. Whereas direct numerical solution of the time-dependent Schrödinger equation (TDSE) can be used for atomic and simple linear molecular targets within the single-active-electron approximation, such an approach is not practical for polyatomic molecules. Thus most of the current calculations for HHG from molecules are still based on simple theories, such as the strong-field approximation (SFA) [18–20], the eikonal-Volkov approximation [11,21], and the quantitative rescattering theory (QRS) [22,23]. Clearly, interpretation of experimental data and the extraction of structure information rely heavily on the accuracy of those theories.

The QRS has proved so far to be quite successful for atomic and simple linear molecules [22,23]. In this paper, we discuss technical issues relevant to the practical applications of the QRS for HHG from polyatomic molecules. Although the main purpose of this paper is to illustrate how the QRS is carried out in a real application for the case of polyatomic molecules, we have additional goals. First, we introduce some simplifications for the treatment of the phase of the electron wave packet. As HHG spectra from some polyatomic molecules contain robust and pronounced minima [15–17], they provide ideal benchmarks with which different theories can be compared. Thus the second goal of this paper is to test our theory against available experimental data on an example molecule, which we take to be  $\text{CCl}_4$ .

This paper is organized as follows. In Sec. II, we briefly describe the QRS theory and discuss practical complications

for the case of polyatomic molecules. We then provide a detailed analysis for the phase of the electron returning wave packet on  $\text{CCl}_4$ , which is our example molecule. Such analysis suggests that an angle-dependent phase needs to be added to the phase of the electron wave packet obtained from the SFA for a reference atom. This additional phase can be approximated by the phase of the asymptotic wave function of the active electron. The method will be illustrated by considering the  $\text{CCl}_4$  molecule in Sec. III, where our results will be compared with data from the experiment by Bhardwaj and collaborators for  $\text{CCl}_4$  [17] for the case of isotropic molecular distribution. In particular, the minimum in HHG spectrum observed in their experiment [17] is well reproduced. We further provide detailed analysis of the origin of this minimum. The effect of molecular alignment dependence and degenerate HOMOs are also discussed. Finally, we give a summary and outlook in Sec. IV.

**II. THEORETICAL METHOD****A. The quantitative rescattering theory**

Although the QRS has been described in detail in Refs. [22,23], in this section we briefly describe the QRS and discuss several technical issues specifically related to polyatomic molecules. We first describe the theory in the molecular frame, in which photoionization is more conveniently calculated. The results can then be converted to the laboratory frame by appropriate transformations. Atomic units are used throughout the paper unless otherwise indicated.

Within the QRS, the complex induced dipole  $D(\omega, \theta, \phi)$  for a molecule in a linearly polarized intense laser pulse is written as a product of a returning electron wave packet  $W(E, \theta, \phi)$  and the transition dipole  $d(\omega, \theta, \phi)$ ,

$$D(\omega, \theta, \phi) = W(E, \theta, \phi)d(\omega, \theta, \phi), \quad (1)$$

where  $\omega$  is the photon energy of the emitted harmonic and  $\theta$  and  $\phi$  are the polar and azimuthal angles, describing the direction of the laser polarization with respect to the  $z$  axis of the molecular frame. Here, the electron energy  $E$  is related to the emitted photon energy  $\omega$  by  $E = \omega - I_p$ , with  $I_p$  being the (vertical) ionization potential of the target. The HHG power spectrum can be calculated from the induced dipole as

$$P(\omega, \theta, \phi) \propto |a(\omega, \theta, \phi)|^2 \approx \omega^4 |D(\omega, \theta, \phi)|^2, \quad (2)$$

where  $a(\omega, \theta, \phi)$  is the induced dipole acceleration. The QRS theory has been well established for atomic and linear molecular targets and has been shown to agree very well with benchmark calculations using the numerical solution of the TDSE [6,24,25] as well as experiments (see Refs. [7,22,23] and references therein for the earlier results and [26–31] for more recent results with the inclusion of the macroscopic propagation).

In practice, transition dipoles can be calculated by using modern molecular photoionization methods. In this paper, we use the EPOLYSCAT package [32] for polyatomic molecules. As for the returning electron wave packet there are two main methods of calculation. First, it can be conveniently and quite accurately calculated by using the SFA. This method was called the QRS1 in Ref. [22]. More specifically,

$$W^{\text{QRS1}}(E, \theta, \phi) = \frac{D^{\text{SFA}}(\omega, \theta, \phi)}{d^{\text{PWA}}(\omega, \theta, \phi)}, \quad (3)$$

where  $D^{\text{SFA}}$  is the induced dipole calculated within the SFA [18] and  $d^{\text{PWA}}$  is the transition dipole in the plane-wave approximation. Second, the wave packet, as a function of energy, has been shown to be nearly independent of the target, except for an overall factor, which is proportional to the ionization rate [6,22,24]. Therefore, for practical purposes, a reference atom of similar ionization potential as the target can be used to extract the returning electron wave packet. This reference atom method was called QRS2 in Ref. [22], which can be written as

$$\begin{aligned} W^{\text{QRS2}}(E, \theta, \phi) &= \left( \frac{N(\theta, \phi)}{N^{\text{ref}}} \right)^{1/2} W^{\text{ref}}(E) e^{i\Delta\eta(E, \theta, \phi)} \\ &= \left( \frac{N(\theta, \phi)}{N^{\text{ref}}} \right)^{1/2} \frac{D^{\text{ref}}(\omega)}{d^{\text{ref}}(\omega)} e^{i\Delta\eta(E, \theta, \phi)}. \end{aligned} \quad (4)$$

Here,  $N$  and  $N^{\text{ref}}$  are the ionization probability for electron emission along the laser polarization direction from the molecule and reference atom, respectively. In practice,  $N$  can be approximated in the tunneling regime as the total ionization probability and can be calculated using the molecular tunneling ionization [molecular Ammosov-Delone-Krainov (MO-ADK)] theory [33].  $\Delta\eta$  is introduced to account for the phase difference between the two wave packets. This phase difference has been shown to be nearly independent of energy [24]. One can calculate  $D^{\text{ref}}$  by solving numerically the TDSE and use it in conjunction with  $d^{\text{ref}}$  from the well-known exact analytical expression for scaled H(1s). Alternatively, one can again use the SFA and plane-wave approximation for  $D^{\text{ref}}$  and  $d^{\text{ref}}$ , respectively, as in the QRS1. We remark that a “reference atom” has been used before in the context of orbital tomography [4,34].

It has been shown that both methods of calculating the returning electron wave packet agree quite well with each other. The SFA method, however, has a serious drawback at times. Indeed, near a Cooper minimum in the plane-wave approximation, where the transition dipole vanishes, the wave packet is undetermined. For example, the transition dipole in the plane-wave approximation from Ar( $3p_0$ ) vanishes near 22 eV, which leads to a spurious spike in the HHG spectra near  $\omega = 22$  eV [22,24]. This could be a minor problem if it occurs outside the energy range of interest. The problem

is more serious for complex polyatomic targets, in which the wave packet depends on the direction of the laser polarization  $\theta$  and  $\phi$ . The reference atom method, on the other hand, does not suffer from this problem. Indeed, for a reference atom one can choose the  $1s$  ground state of a scaled “hydrogenlike” atom, in which the nuclear charge is chosen so that the atom has the same ionization potential as the target. In this case there are no zeros in the transition dipole. This method further requires knowledge of the ionization rate. However, the additional phase of the wave packet  $\Delta\eta$ , as a function of angles, is largely unknown (except for simple linear molecules; see the next section). This would not be an issue in the case of perfectly aligned molecules and when one is only interested in HHG intensity. In real experiments, molecules can only be partially aligned or even nonaligned. Since HHG induced dipoles need to be added up coherently from different alignment angles, one needs to know their relative phase for different alignment angles. Although our theory is applicable to aligned polyatomic molecules, in this paper we consider only the nonaligned (isotropic) case, which is of interest for recent experiments (see, for example, [15–17]). In this case the alignment-averaged induced dipole can be written as

$$\bar{D}(\omega) = \frac{1}{4\pi} \int_0^\pi d\theta \int_0^{2\pi} d\phi D(\omega, \theta, \phi) \sin\theta. \quad (5)$$

In the next section, we provide a detailed analysis for the phase of the wave packet from polyatomic targets.

## B. Phase of the returning wave packet

As can be seen from Eq. (3), the phase of the returning wave packet  $W$  can be calculated explicitly, except at the singularities where the transition dipole vanishes in the plane-wave approximation. Since the phase is less sensitive to the singularities, in comparison to the amplitude, it can be smoothed out by using appropriate interpolation procedures. The smooth phase, as a function of angles, can then be used together with the wave-packet amplitude from a reference atom in Eq. (4). In this section we show that the phase can be more conveniently approximated by using the asymptotic molecular orbital wave function of the active electron. We will demonstrate our procedure for the case of the  $\text{CCl}_4$  molecule.

The  $\text{CCl}_4$  molecule ( $T_d$  symmetry group) has a triply degenerate ( $2t_1$ ) HOMO, with an ionization potential  $I_p = 11.47$  eV. Induced dipoles from degenerate HOMOs are added up coherently [19]. For illustration purposes, we can therefore limit ourselves to one HOMO. Since the other HOMOs can be obtained by appropriate rotations, the HHG from the degenerate HOMOs should be identical to each other in the case of nonaligned  $\text{CCl}_4$ .

In Fig. 1(a) we show a color-coded plot of the asymptotic wave function for one of the degenerate HOMOs (denoted HOMO1 in the following). For convenience in the following analysis, the wave function is plotted as a function of spherical angles  $\theta = \pi - \theta_e$  and  $\phi = \phi_e + \pi$ , where  $\theta_e$  and  $\phi_e$  are the electron azimuthal and polar angles, respectively, defined with respect to the molecular frame. This reversed direction ( $\mathbf{r}_e \rightarrow -\mathbf{r}$ ) is used since the electron (a negative charge particle) tunnels in the opposite direction of the electric field. The HOMOs are first calculated by using the Gaussian quantum

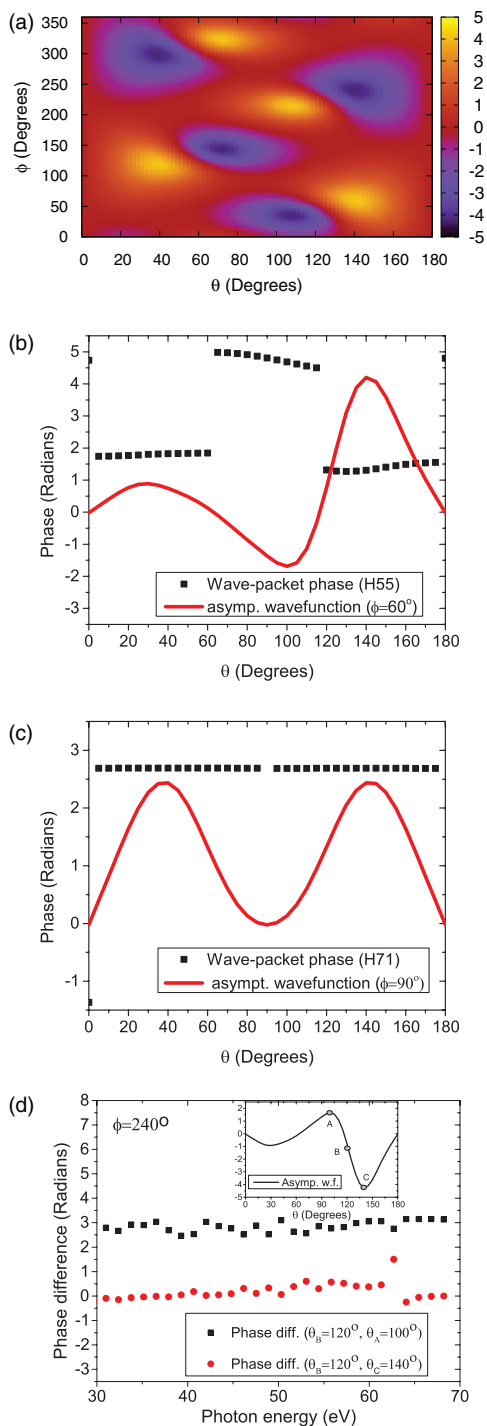


FIG. 1. (Color online) (a) Asymptotic wave function of a HOMO (denoted as HOMO1) of  $\text{CCl}_4$ . (b) Phase of the returning electron wave packet for H55 at  $\phi = 60^\circ$ . The asymptotic wave function at  $\phi = 60^\circ$  is also shown (red line). (c) Same as (b), but for H71 and the asymptotic wave function at  $\phi = 90^\circ$ . (d) Wave-packet phase difference between  $\theta_A = 100^\circ$  and  $\theta_B = 120^\circ$  (points A and B in the inset) and between  $\theta_B = 120^\circ$  and  $\theta_C = 140^\circ$  (points B and C in the inset). Here  $\phi$  is fixed at  $240^\circ$ . The inset shows the asymptotic wave function.

chemistry code [35]. We use the augmented correlation-consistent polarized valence triple-zeta (aug-cc-pVTZ) basis set at the Hartree-Fock level. These HOMOs are then used to extract the asymptotic limit in the same manner as in the

molecular tunneling ionization theory (MO-ADK) [33,36]. This procedure is typically done at  $r \approx 10$  a.u.

We show in Fig. 1(b) the phase of the wave packet for 55th harmonic (or H55) as functions of  $\theta$  for fixed  $\phi = 60^\circ$ . The calculation was done by using Eq. (3) with an 1800-nm wavelength laser pulse with an intensity of  $0.55 \times 10^{14} \text{ W/cm}^2$  and 40-fs pulse duration. We also plot in Fig. 1(b) the phase of the asymptotic wave function at this fixed  $\phi$ . It is clear that the phase of the wave packet is nearly unchanged with  $\theta$ , except for some abrupt jumps by  $\pi$ , which are associated with the phase jumps in the asymptotic wave function. Another example is shown in Fig. 1(c) for H71 at  $\phi = 90^\circ$  under the same laser pulse. In this case, the phase is unchanged except near  $\theta = 90^\circ$ , where the wave function is very small. Similar behavior is observed for other harmonics.

The above results suggest that the phase of the asymptotic wave function can be used, up to a constant (orientation independent) shift, as an approximation to the “extra” phase of the returning wave packet in the reference atom approach. We found that the phase of the wave packet is more angle dependent near directions where the asymptotic wave function is small. This does not cause much problem for our approximation in general since the tunneling ionization (and therefore the wave packet) is weak for those directions.

To further illustrate our approximation, we show in Fig. 1(d) the phase difference between the wave packets at  $\{\theta_A = 100^\circ, \phi = 240^\circ\}$  and  $\{\theta_B = 120^\circ, \phi = 240^\circ\}$  (points A and B in the inset) as a function of harmonic order. The phase difference is nearly  $\pi$  for all harmonics, although the phase itself varies quickly as a function of energy (or harmonic order). This is the case when the asymptotic wave function has the opposite phase in the two directions (see the inset). This is in contrast to the phase difference between the wave packets at  $\{\theta_B = 120^\circ, \phi = 240^\circ\}$  and  $\{\theta_C = 140^\circ, \phi = 240^\circ\}$  (points B and C in the inset), which is close to zero, as the asymptotic wave function has the same phase in these two directions (see the inset). This indicates that the phases for different harmonics are “locked” to each other. In other words, they are different by some phase shift (see the previous paragraph), which can be obtained from the SFA for a chosen direction or for a reference atom. In practice it is therefore more convenient to use the wave packet from the reference atom approach [Eq. (4)], with the additional phase  $\Delta\eta$  from the phase of the asymptotic wave function. As can be seen from Eq. (4), the origin of this additional phase is due to the missing phase in the ionization probability amplitude. Within this approximation, there is no need to carry out any interpolation to smooth out the possible spurious spikes in the amplitude and phase of the wave packet, which are difficult to control in the standard approach [Eq. (3)].

We note that for simple linear molecules studied before using QRS such as  $\text{N}_2$ ,  $\text{O}_2$ , and  $\text{CO}_2$ , the phase of the wave packet for any harmonic is nearly the same for  $\theta = [0, \pi/2]$ . For  $\theta = [\pi/2, \pi]$  this phase remains the same for  $\text{N}_2$  (with the HOMO in  $\sigma_g$ ) and experiences a jump by  $\pi$  at  $\theta = \pi/2$  for  $\text{O}_2$  and  $\text{CO}_2$  (both with the HOMO in  $\pi_g$ ) due to symmetry, as can also easily be seen from the HOMOs (not shown). For completeness, we remark that the transition dipole  $d(\omega, \theta)$  from the HOMO for both  $\text{O}_2$  and  $\text{CO}_2$  also experiences a phase jump by  $\pi$  at  $\theta = \pi/2$ . The complex induced dipole [see Eq. (1)] therefore does not experience any phase jump. In fact,

$D(\omega, \theta) = D(\omega, \pi - \theta)$ , and the averaging over the alignment distribution can be carried out for  $\theta = [0, \pi/2]$  only, as can be expected from symmetry considerations. We refer readers to Refs. [4, 12, 13] for previous treatment of the phase of the wave packet in the case of linear molecules in the context of orbital tomography. The situation is more complicated for polyatomic molecules, as can be seen in Fig. 1(a) for the case of  $\text{CCl}_4$ .

### III. RESULTS

#### A. Molecular frame treatment: Case of perfectly aligned $\text{CCl}_4$

In this section, we show the application of our method for the case of  $\text{CCl}_4$ . This molecule is of interest since it has been shown quite recently as an example when HHG spectra show the influence of the Cooper-type minimum in photoionization cross section (PICS) [17]. We start with the treatment in the molecular frame for the case of fixed-in-space molecules. In the case of partial molecular alignment (although not applicable to this particular molecule), averaging over the alignment distribution should be carried out for complex induced dipoles from all degenerate HOMOs.

First, we show the real and imaginary parts of the transition dipole in Figs. 2(a) and 2(b), respectively, for a photon energy of 54.4 eV (or H79 for the case of an 1800-nm wavelength) as functions of the laser polarization direction. Note that within the QRS, only an electron that was emitted along this direction and returned back to the parent ion contributes to

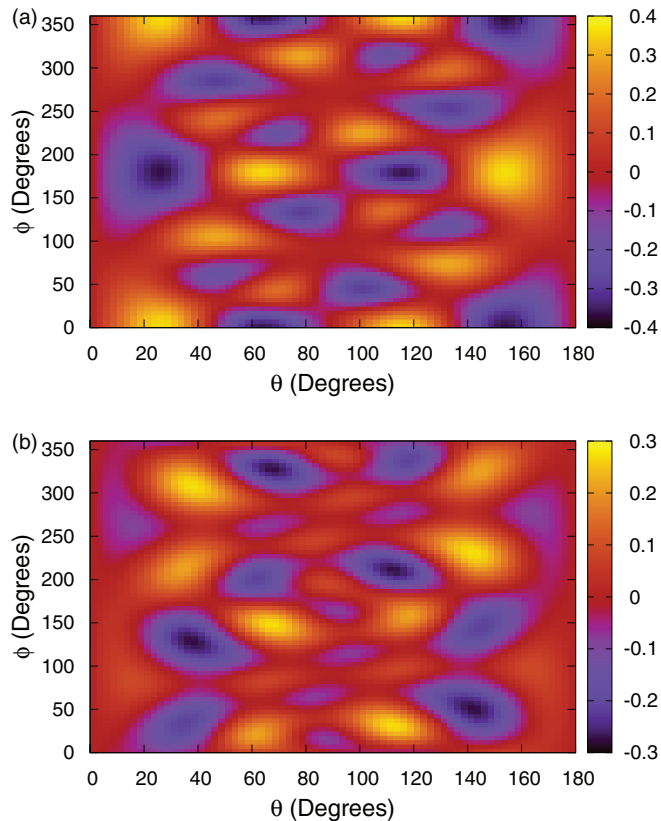


FIG. 2. (Color online) (a) Real and (b) imaginary parts of the photoionization transition dipole from HOMO1 of  $\text{CCl}_4$  at a photon energy of 54.4 eV vs the laser polarization direction (or the electron emission direction)  $\Omega = \{\theta, \phi\}$ .

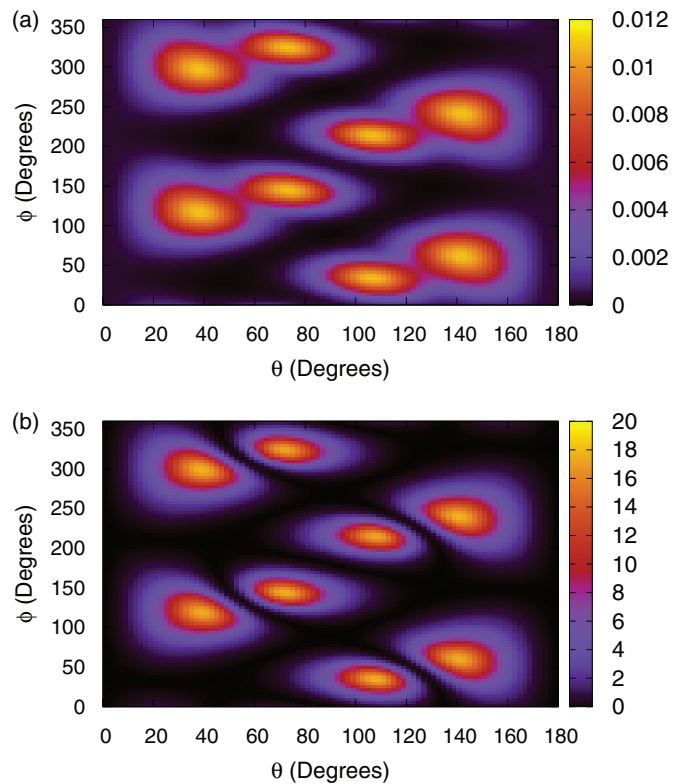


FIG. 3. (Color online) (a) Ionization rate from HOMO1 of  $\text{CCl}_4$  vs the laser polarization direction, calculated by the MO-ADK theory [33] for a laser intensity of  $0.55 \times 10^{14} \text{ W/cm}^2$ . (b) Asymptotic electron density for HOMO1 of  $\text{CCl}_4$ . See text for more details.

the HHG process [22]. The calculation was carried out with the state-of-the-art molecular photoionization code EPOLYSCAT [32]. The transition dipole shows much more complicated structures compared to the typical diatomic molecules such as  $\text{N}_2$  and  $\text{O}_2$  [22]. The ionization rate, calculated within the MO-ADK theory [33], is presented in Fig. 3(a) for a laser intensity of  $0.55 \times 10^{14} \text{ W/cm}^2$ . We also show in Fig. 3(b) the probability density of the asymptotic wave function. For Fig. 3(b), angles  $\theta$  and  $\phi$  are defined in the same way as in Fig. 1(a) (see discussion in Sec. II B). Clearly, the ionization rate resembles closely the asymptotic probability density, as has been noted before (see, for example, Zhao *et al.* [36]). In this respect, it is not entirely surprising that the missing phase for the ionization probability amplitude in Eq. (4) can be approximated by the phase of the asymptotic wave function. A typical amplitude of the wave packet, calculated from Eq. (4) with a reference hydrogenlike atom, is shown in Fig. 4(a). The calculation was performed for the case of an 1800-nm wavelength laser pulse with an intensity of  $0.55 \times 10^{14} \text{ W/cm}^2$  and a 40-fs pulse duration.

With all the ingredients for the QRS theory in place, we can now calculate the HHG spectrum by using Eq. (1). First, we show in Fig. 4(b) HHG spectra from HOMO1 for different laser polarizations  $\theta = 30^\circ, \phi = 110^\circ$ ;  $\theta = 65^\circ, \phi = 140^\circ$ ; and  $\theta = 110^\circ, \phi = 10^\circ$ . We note that the shapes and magnitudes of the spectra are quite different. In particular, there is a quite pronounced minimum near 40 eV for  $\theta = 30^\circ, \phi = 110^\circ$ . This minimum is shifted quite significantly up to 48 eV for

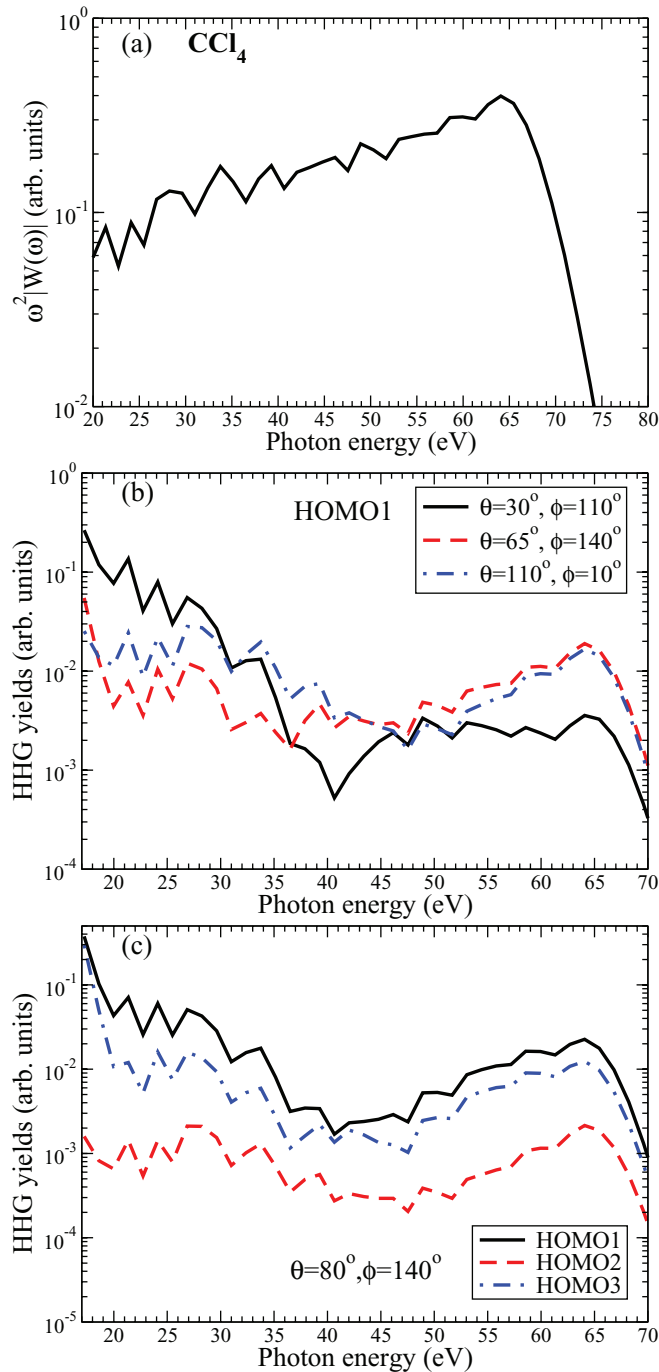


FIG. 4. (Color online) (a) Amplitude (scaled by  $\omega^2$ ) of the returning electron wave packet vs emitted photon energy  $\omega$  for a typical case of an 1800-nm wavelength laser pulse with an intensity of  $0.55 \times 10^{14}$  W/cm<sup>2</sup> and a 40-fs pulse duration. (b) HHG spectra from HOMO1 for different laser polarization directions (as shown in the legend). (c) HHG spectra for a fixed laser polarization direction (or fixed molecular alignment) at  $\theta = 80^\circ, \phi = 140^\circ$  from the three degenerate HOMOs. Only envelopes (odd harmonics) are shown.

$\theta = 110^\circ, \phi = 10^\circ$  and down to near 36 eV and becomes quite shallow for  $\theta = 65^\circ, \phi = 140^\circ$ . Clearly, these differences reflect the changes in the transition dipole as a function of photon energy and angles (also see Figs. 2 and 7). These spectra cannot be observed experimentally. Instead, HHG yields from

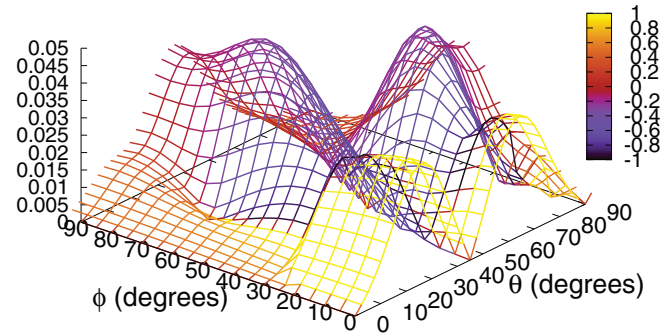


FIG. 5. (Color online) Induced dipole amplitude (vertical axis) and phase (color code) for H79 (photon energy of 54.4 eV) from HOMO1 of  $\text{CCl}_4$  vs the laser polarization direction  $\Omega = \{\theta, \phi\}$ . The phase is given in units of  $\pi$  rad. Laser parameters are the same as in Fig. 4.

all three degenerate HOMOs of  $\text{CCl}_4$  are added up coherently. In Fig. 4(c) we show the contribution from each HOMO for a fixed polarization direction at  $\theta = 80^\circ, \phi = 140^\circ$ . Clearly, interference from these contributions is expected due to the differences in the amplitude and phase of the induced dipoles for a fixed polarization direction (not shown). We remark that these degenerate HOMOs of  $\text{CCl}_4$  can be obtained from one another by appropriate rotations. Therefore, averaging the HHG yield from any one of the degenerate HOMOs over an isotropic distribution is expected to yield a result that is identical to that obtained from the others (see next the section).

Apart from the interference due to degenerate HOMOs, interference from different alignment angles is expected to be significant in polyatomic molecules. Here we use  $\text{CCl}_4$  to further illustrate this point, although laser-induced alignment is not applicable to this molecule. We show in Fig. 5 the amplitude and phase of the induced dipole from HOMO1 at a photon energy of 54.4 eV (H79) as functions of laser polarization direction. The rapid changes in phase with polarization (or alignment) direction seen in Fig. 5 suggest that, depending on the alignment angles, the constructive (or destructive) interference effect could be very dramatic in the case of partially aligned molecules. It would be of great interest to observe this kind of interference from polyatomic molecules in future experiments.

### B. Case of isotropic molecular distribution and the nature of the Cooper-type minimum in $\text{CCl}_4$

In general, the HHG induced dipoles for all three degenerate HOMOs need to be added up coherently. In the case of the nonaligned molecules, we have checked that the HHG yields from the degenerate HOMOs are identical to each other after averaging over the isotropic distribution using Eq. (5), as expected. The result of this averaging is presented in Fig. 6. One can easily see the pronounced minimum in the spectrum near 41 eV. This minimum can be associated with the Cooper-type minimum in the calculated photoionization cross section, found near 48 eV using EPOLYSCAT [see Fig. 9(a) below]. The experimental observed minimum in the photoionization cross section is near 43 eV [37]. In fact, the minimum is quite stable with respect to the laser intensity and wavelength. As

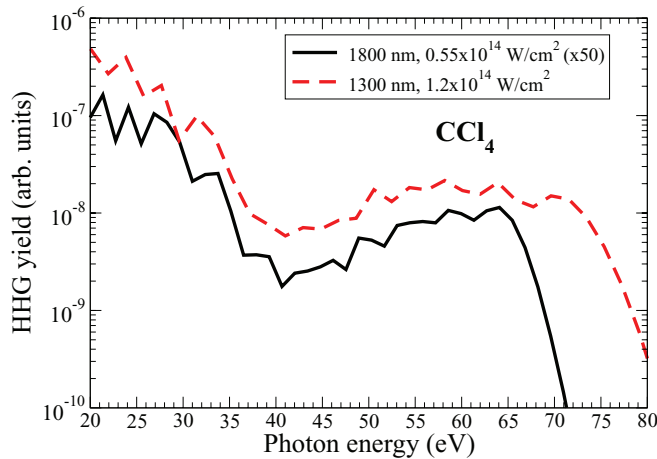


FIG. 6. (Color online) HHG spectra from  $\text{CCl}_4$  for different laser pulses for the case of isotropic molecular distribution. Laser parameters are given in the text. The yield from an 1800-nm laser pulse (black line) has been multiplied by a factor of 50. Only envelopes are shown.

an example, we also show in Fig. 6 the HHG spectrum for the case of a 1300-nm wavelength laser pulse with an intensity of  $1.2 \times 10^{14} \text{ W/cm}^2$  and a pulse duration of 40 fs. Although the calculation is done for the single molecule response, we expect this pronounced minimum to survive after the macroscopic propagation is carried out.

Compared to the experimental data by Wong *et al.* [17], the theoretical result shows a slightly deeper minimum. This is probably due to the fact that the macroscopic propagation can suppress HHG yields near the cutoff. This is especially true for the case of the midinfrared laser of relatively high laser intensity used in the experiment due to the modification of the driving laser pulse in the medium [38]. This conclusion is further supported by the fact that the experimental laser intensity estimate is  $9 \times 10^{13} \text{ W/cm}^2$ , significantly higher than the theoretical estimate of  $0.55 \times 10^{14} \text{ W/cm}^2$ , based on the position of the cutoff. The discrepancies at lower energies could be partly due to the absorption of the HHG by the medium, which is neglected in the single molecular response. It has been shown, for example, by Wang *et al.* [39] that absorption tends to suppress HHG yield more strongly at lower energies.

In order to understand the origin of the minimum in HHG spectra, we now analyze the transition dipole. We show in Figs. 7(a)–7(c), the transition dipole amplitude  $|d(\omega, \theta, \phi)|$  at different photon energies of 41, 48, and 60 eV, respectively. Although the shape is slightly changed in this energy range as energy increases, as a whole the transition dipole appears to have a minimum near 48 eV (see the color scale). This is exactly the location of the Cooper-type minimum in the theoretical total PICS (after averaging over the alignment and photoelectron distribution), obtained from EPOLYSCAT [see Fig. 9(a) below]. Note that within the QRS, only the electron emitted along the laser polarization direction contributes to the HHG process. On the other hand, the theoretical minimum in HHG spectra occurs near 41 eV [see Fig. 4(b)]. This shift to a lower energy is partly due to the positive slope of the wave packet as a function of energy, as shown in Fig. 4(a).

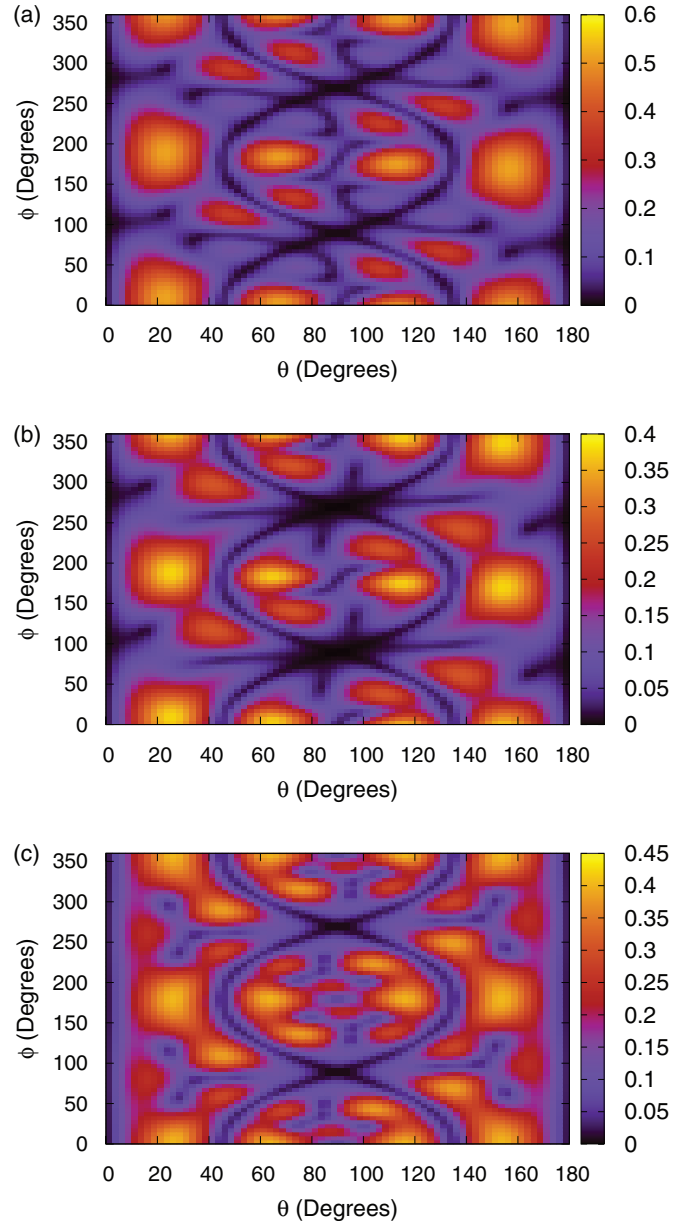


FIG. 7. (Color online) Transition dipole amplitude for  $\text{CCl}_4$  at a photon energy of (a) 41 eV, (b) 48 eV, and (c) 60 eV vs the laser polarization direction.

The analysis of the case of  $\text{CCl}_4$  is rather simple, as the angular dependence of the PICS only slightly changes with energy near the position of the Cooper-type minimum. In general, however, the angular dependence of both the amplitude and phase of the transition dipole and their overlap with the ionization rate varies with energy, so the appearance of any structure in a HHG spectrum needs to be analyzed carefully. Constructive or destructive interference from different directions can, in principle, greatly affect the shape of the observed HHG spectra. This type of interference is expected to be even more dramatic for aligned molecules, as discussed in the previous section.

To further illustrate this issue, we compare in Fig. 8 theoretical spectra from (nonaligned)  $\text{CCl}_4$ ,  $\text{trans-C}_2\text{H}_2\text{Cl}_2$ , and  $\text{CH}_4$ . The data have been shifted vertically for clarity.

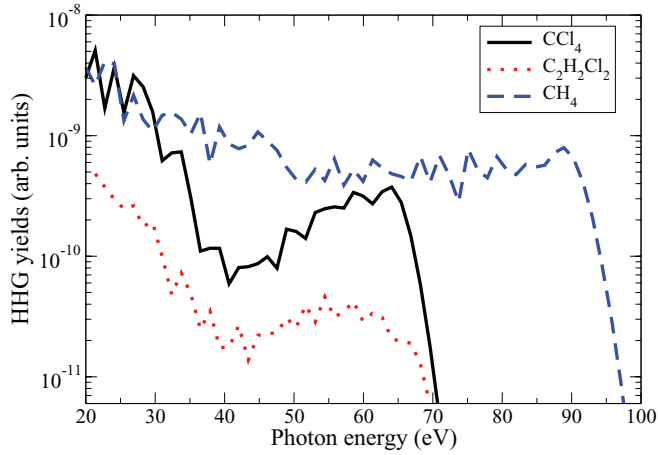


FIG. 8. (Color online) Theoretical HHG spectra from  $\text{CCl}_4$ , trans- $\text{C}_2\text{H}_2\text{Cl}_2$ , and  $\text{CH}_4$ . Results have been shifted vertically for clarity. Only envelopes are shown.

We see a shallow minimum near 44 eV in the spectrum from trans- $\text{C}_2\text{H}_2\text{Cl}_2$ , although there is no clear evidence of the Cooper-type minimum in the total PICS (after averaging over the alignment and photoelectron distribution). However, the angular dependence of the transition dipole changes quite significantly near the observed HHG minimum. Experiments by Bhardwaj's group [16,17] found a Cooper-type minimum in HHG spectra near 43 eV, which is quite stable with respect to laser parameters. Finally, the spectrum from  $\text{CH}_4$  shows no obvious minimum. Its PICS (not shown) has no minimum, and the angular dependence of the transition dipole is nearly unchanged in the range of energy under consideration. There is no obvious minimum seen in the experimental HHG spectra using midinfrared laser pulses [40,41]. Note that for  $\text{CH}_4$  we have used an 1800-nm wavelength laser pulse with an intensity of  $0.8 \times 10^{14} \text{ W/cm}^2$  to explore a more extended plateau.

### C. On the possibility of extracting PICS from HHG spectra for nonaligned polyatomic molecules

HHG spectra carry information about the photorecombination process (or its time-inverse process, photoionization) [6,7,22,23,42]. In fact, it has been shown that the *differential* photoionization or photorecombination cross section and the dipole phase can be extracted from HHG spectra for atomic targets and aligned diatomic molecules (see, for example, [6,8,10,24,43]). The question is, can one extract the *total* (i.e., integrated over all emission directions and the polarization direction) PICS from an HHG spectrum of nonaligned molecules by a simple procedure using a reference atom, as has been done in Refs. [6,8]? This question is of interest since total PICS is normally measured in the molecular photoionization experiments. By combining Eqs. (1), (2), (4), and (5) within the reference atom approach, the HHG power spectrum for nonaligned molecules can be written as

$$\overline{P}(\omega) = \left| \omega^2 W^{\text{ref}}(\omega) \int_0^\pi \sin \theta d\theta \int_0^{2\pi} d\phi \times N^{1/2}(\theta, \phi) e^{i\Delta\eta(\omega, \theta, \phi)} d(\omega, \theta, \phi) \right|^2. \quad (6)$$

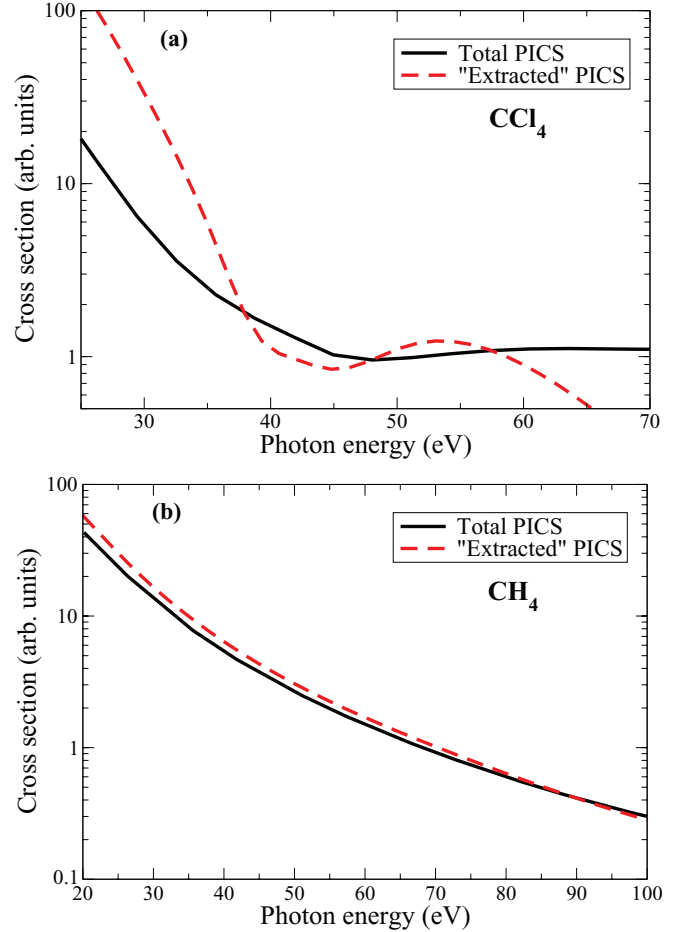


FIG. 9. (Color online) Extracted total photoionization “cross section” from HHG spectra for (a)  $\text{CCl}_4$  and (b)  $\text{CH}_4$ . The theoretical total PICS calculated by the EPOLYSCAT code [32] are also shown.

It is clear from Eq. (6) that from an HHG spectrum of nonaligned molecules one can only extract the angle-averaged cross section weighted by the angle-dependent complex tunneling ionization amplitude. Furthermore, this cross section contains only information for the electron emission direction along the laser polarization, whereas in the total PICS, averaging over the emission direction is carried out. We therefore do not expect, in general, the result of this simple extraction procedure to agree with the total PICS. In Fig. 9(a) we show the comparison for the weighted cross section, extracted from the HHG spectrum, together with the theoretical total PICS for  $\text{CCl}_4$ , calculated by EPOLYSCAT [32]. The laser parameters are the same as in Fig. 3. They do not agree with each other, as expected. On the other hand, we have observed situations when the two agree. As an example we show in Fig. 9(b) a comparison for the case of  $\text{CH}_4$ . Surprisingly, the extracted PICS agrees quite well with the theoretical one.

## IV. SUMMARY AND OUTLOOK

In this paper we have discussed various technical issues related to the practical application of the quantitative rescattering theory as applied to the HHG process from polyatomic molecules. A major simplification presented in this paper

is for the treatment of the phase of the returning wave packet, used in the reference atom approach. The conceptual simplicity of this method should be useful for developing intuitive understanding of the HHG process. Furthermore, such a simplification is important for the efficiency of any realistic simulations of HHG from polyatomic targets since macroscopic propagation still needs to be carried out. For a typical macroscopic propagation, calculations at hundreds or thousands of laser intensities in the interaction volumes are needed.

We have also presented an application of our theory to  $\text{CCl}_4$ . Our results agree well with available experiments. In particular, the minimum in HHG spectra observed in  $\text{CCl}_4$  by the Bhardwaj group [17] is well reproduced in our theory. Within the QRS, the origin of these minima can be traced back to the photorecombination (or photoionization) transition dipole. The presence of structures in HHG spectra is of great significance for the understanding of target structures, and it can also serve as a benchmark for different theories. This is even more so for the Cooper-type minima, which are robust with respect to laser parameters, compared to

the other dynamic structures. Strictly speaking, the QRS is applicable only in the tunneling regime (when the Keldysh parameter is close to 1 [1,22]). In this paper we have not included the depletion of the ground state. Although it can be incorporated into the QRS, the accuracy of the QRS has not been documented for the case when depletion is significant. In this regard we remark that the MO-ADK and SFA ionization rates used in the QRS are also questionable in this regime, in particular, in over-barrier ionization. While the agreement with current experiments is encouraging for the QRS, it would be interesting to see how the QRS performs in even more severe tests in the future. With ultrafast intense midinfrared laser sources becoming available, future HHG experiments with aligned polyatomic molecules are extremely desirable.

#### ACKNOWLEDGMENTS

We thank V. R. Bhardwaj for stimulating discussions. This work was supported in part by the Chemical Sciences, Geosciences and Biosciences Division, Office of Basic Energy Sciences, Office of Science, US Department of Energy.

- 
- [1] F. Krausz and M. Ivanov, *Rev. Mod. Phys.* **81**, 163 (2009).
- [2] T. Popmintchev, M. C. Chen, P. Arpin, M. M. Murnane, and H. C. Kapteyn, *Nat. Photonics* **4**, 822 (2010).
- [3] G. Sansone, E. Benedetti, F. Calegari, C. Vozzi, L. Avaldi, R. Flammini, L. Poletto, P. Villoresi, C. Altucci, R. Velotta, S. Stagira, S. De Silvestri, and M. Nisoli, *Science* **314**, 443 (2006).
- [4] J. Itatani, J. Levesque, D. Zeidler, H. Niikura, H. Pepen, J. C. Kiefer, P. B. Corkum, and D. M. Villeneuve, *Nature (London)* **432**, 867 (2004).
- [5] M. Lein, *J. Phys. B* **40**, R135 (2007).
- [6] T. Morishita, A. T. Le, Z. Chen, and C. D. Lin, *Phys. Rev. Lett.* **100**, 013903 (2008).
- [7] A. T. Le, R. R. Lucchese, M. T. Lee, and C. D. Lin, *Phys. Rev. Lett.* **102**, 203001 (2009).
- [8] S. Minemoto, T. Umegaki, Y. Oguchi, T. Morishita, A. T. Le, S. Watanabe, and H. Sakai, *Phys. Rev. A* **78**, 061402(R) (2008).
- [9] B. K. McFarland, J. P. Farrell, P. H. Bucksbaum, and M. Gühr, *Science* **322**, 1232 (2008).
- [10] W. Boutu, S. Haessler, H. Merdji, P. Breger, G. Waters, M. Stankiewicz, L. J. Frasinski, R. Taieb, J. Caillat, A. Maquet, P. Monchicourt, B. Carre, and P. Salieres, *Nat. Phys.* **4**, 545 (2008).
- [11] O. Smirnova, Y. Mairesse, S. Patchkovskii, N. Dudovich, D. Villeneuve, P. Corkum, and M. Yu. Ivanov, *Nature (London)* **460**, 972 (2009).
- [12] S. Haessler, J. Caillat, W. Boutu, C. Giovanetti-Teixeira, T. Ruchon, T. Auguste, Z. Diveki, P. Breger, A. Maquet, B. Carre, R. Taieb, and P. Salieres, *Nat. Phys.* **6**, 200 (2010).
- [13] C. Vozzi, M. Negro, F. Calegari, G. Sansone, M. Nisoli, S. De Silvestri, and S. Stagira, *Nat. Phys.* **7**, 822 (2011).
- [14] R. Torres, N. Kajumba, J. G. Underwood, J. S. Robinson, S. Baker, J. W. G. Tisch, R. de Nalda, W. A. Bryan, R. Velotta, C. Altucci, I. C. E. Turcu, and J. P. Marangos, *Phys. Rev. Lett.* **98**, 203007 (2007).
- [15] M. C. H. Wong, J.-P. Brichta, and V. R. Bhardwaj, *Phys. Rev. A* **81**, 061402(R) (2010).
- [16] M. C. H. Wong, J.-P. Brichta, M. Spanner, S. Patchkovskii, and V. R. Bhardwaj, *Phys. Rev. A* **84**, 051403 (2011).
- [17] M. C. H. Wong, A. T. Le, A. F. Alharbi, A. E. Boguslavskiy, R. R. Lucchese, J.-P. Brichta, C. D. Lin, and V. R. Bhardwaj, *Phys. Rev. Lett.* **110**, 033006 (2013).
- [18] M. Lewenstein, Ph. Balcou, M. Yu. Ivanov, A. L'Huillier, and P. B. Corkum, *Phys. Rev. A* **49**, 2117 (1994).
- [19] C. B. Madsen and L. B. Madsen, *Phys. Rev. A* **76**, 043419 (2007).
- [20] S. Odzak and D. B. Milosevic, *Phys. Rev. A* **79**, 023414 (2009).
- [21] O. Smirnova, M. Spanner, and M. Ivanov, *Phys. Rev. A* **77**, 033407 (2008).
- [22] A. T. Le, R. R. Lucchese, S. Tonzani, T. Morishita, and C. D. Lin, *Phys. Rev. A* **80**, 013401 (2009).
- [23] C. D. Lin, A. T. Le, Z. Chen, T. Morishita, and R. R. Lucchese, *J. Phys. B* **43**, 122001 (2010).
- [24] A. T. Le, T. Morishita, and C. D. Lin, *Phys. Rev. A* **78**, 023814 (2008).
- [25] A. T. Le, R. D. Picca, P. D. Fainstein, D. A. Telnov, M. Lein, and C. D. Lin, *J. Phys. B* **41**, 081002 (2008).
- [26] A. T. Le, R. R. Lucchese, and C. D. Lin, *Phys. Rev. A* **82**, 023814 (2010).
- [27] C. Jin, A. T. Le, and C. D. Lin, *Phys. Rev. A* **83**, 023411 (2011).
- [28] C. Jin, H. J. Woerner, V. Tosa, A. T. Le, J. B. Bertrand, R. R. Lucchese, P. B. Corkum, D. M. Villeneuve, and C. D. Lin, *J. Phys. B* **44**, 095601 (2011).
- [29] C. Jin, A. T. Le, and C. D. Lin, *Phys. Rev. A* **83**, 053409 (2011).
- [30] A. T. Le and C. D. Lin, *J. Mod. Opt.* **58**, 1158 (2011).
- [31] C. Jin, J. B. Bertrand, R. R. Lucchese, H. J. Woerner, P. B. Corkum, D. M. Villeneuve, A. T. Le, and C. D. Lin, *Phys. Rev. A* **85**, 013405 (2012).

- [32] A. P. P. Natalense and R. R. Lucchese, *J. Chem. Phys.* **111**, 5344 (1999).
- [33] X. M. Tong, Z. X. Zhao, and C. D. Lin, *Phys. Rev. A* **66**, 033402 (2002).
- [34] J. Levesque, D. Zeidler, J. P. Marangos, P. B. Corkum, and D. M. Villeneuve, *Phys. Rev. Lett.* **98**, 183903 (2007).
- [35] M. J. Frisch *et al.*, GAUSSIAN 03, revision C.02, Gaussian Inc., Pittsburgh, PA, 2003.
- [36] S. F. Zhao, J. Xu, C. Jin, A. T. Le, and C. D. Lin, *J. Phys. B* **44**, 035601 (2011).
- [37] T. A. Carlson, M. O. Krause, F. A. Grimm, P. Keller, and J. W. Taylor, *J. Chem. Phys.* **77**, 5340 (1982).
- [38] C. Trallero-Herrero, C. Jin, B. Schmidt, A. Shiner, D. M. Villeneuve, P. B. Corkum, C. D. Lin, F. Legare, and A. T. Le, *J. Phys. B* **45**, 011001 (2012).
- [39] G. Wang, C. Jin, A. T. Le, and C. D. Lin, *Phys. Rev. A* **84**, 053404 (2011).
- [40] P. Wei, C. Liu, C. Zhang, Y. Huang, Y. Leng, P. Liu, Y. Zheng, Z. Zeng, R. Li, and Z. Xu, *Opt. Express* **18**, 11664 (2010).
- [41] C. Trallero-Herrero (private communication).
- [42] M. V. Frolov, N. L. Manakov, T. S. Sarantseva, and A. F. Starace, *Phys. Rev. A* **83**, 043416 (2011).
- [43] X. Ren, V. Makhija, A. T. Le, J. Tross, S. Mondal, C. Jin, V. Kumarappan, and C. Trallero-Herrero (unpublished).